Sensors and Actuators B 247 (2017) 830–839

Contents lists available at ScienceDirect

Sensors and Actuators B: Chemical

journal homepage: www.elsevier.com/locate/snb

Development of a bioelectrode fabricated with a multilayer thin film of poly(diallyldimethylammonium)/gold-nanoparticle/lactate oxidase for analysis of L-lactate in food samples

Verónica I. Paz Zanini[a,*], Omar E. Linarez Pérez[b], Manuel López Teijelo[b], Pierre Labbé[c,d], Beatriz A. Lopez de Mishima[a], Claudio D. Borsarelli[a,*]

[a] Instituto de Bionanotecnología del NOA (INBIONATEC), Universidad Nacional de Santiago del Estero (UNSE), CONICET, RN9, km 1125, G4206XCP, Santiago del Estero, Argentina
[b] Instituto de Investigaciones en Fisicoquímica de Córdoba (INFIQC), Depto. de Fisicoquímica, Facultad de Ciencias Químicas, Universidad Nacional de Córdoba (UNC), Haya de la Torre y Medina Allende, X5000HUA, Córdoba, Argentina
[c] Université Grenoble Alpes, DCM UMR 5250, F-38000, Grenoble, France
[d] CNRS, DCM UMR 5250, F-38000, Grenoble, France

ARTICLE INFO

Article history:
Received 8 November 2016
Received in revised form 23 February 2017
Accepted 18 March 2017
Available online 21 March 2017

Keywords:
Lactate oxidase
Self-assembled multilayers
Gold nanoparticles
Cationic polyelectrolyte

ABSTRACT

Multilayer films made of poly(diallyldimethylammonium) (PDDA), gold nanoparticles (AuNP) of 10 nm diameter and lactate oxidase (LOx), were built for the first time, by layer-by-layer (LBL) assembly technique onto both quartz and gold substrates. The surface plasmon resonance (SPR) band of AuNP was used for monitoring the film growth and adsorption kinetics on PDDA monolayer supported onto quartz substrate. In the case of polycrystalline gold surfaces, electrochemical characterization was performed by means of cyclic voltammetry (CV) and electrochemical impedance spectroscopy (EIS). The latter system was used as bioelectrode for L-lactate quantification, showing a short time response (<10 s) with high sensitivity of $63 \pm 3\ \mu A\ mM^{-1} cm^{-2}$, detection limit of 0.47 μM and linear range between 0.001 mM and 0.25 mM. This bioelectrode was also tested for L-lactate analysis in yogurt and fermented milk, and it was checked that typical interfering as glucose and citric, acetic and ascorbic acids do not play a role. Present results indicate that self-assembled multilayers made of PDDA/AuNP/LOx are suitable thin films for electroanalytical determination of L-lactate in real samples.

1. Introduction

The quantification of L-lactate is of great importance not only in clinical field since it is associated with cellular derangements but also in food industry given that it is linked to stability, storage quality and freshness in dairy products, sausages, wines, fruits and juices [1,2], and to the monitoring of fermentative processes [3]. A wide variety of analytical techniques, such as liquid and ion exclusion chromatography and capillary electrophoresis, have been typically used for the analysis of lactic acid [4–6]. Although highly accurate, most of these techniques are often time-consuming and require laborious sample treatment, expensive instrumentation and highly trained personnel. Additionally, the development of biosensors with L-lactate oxidase (LOx) immobilized onto electro-active surfaces is of great interest for routine analysis of L-lactate in real samples due to several advantages, such as high specificity, rapid response, low cost, portability, and potential for miniaturization and direct assessment [2,7]. Hence, lactate biosensor technology is a field of current development and several approaches has been recently applied in different research areas [2,8,9]. Most of these devices are based on the enzymatic oxidation of L-lactate to pyruvate, where the reduced enzyme species $(LOx)_{red}$ is oxidized by a natural mediator (M) as molecular oxygen (O_2), or artificial mediators (e.g. ferrocene methanol [10] or tetrathiafulvalene [11]), being the electroanalytical signal given by the oxidation of the M_{red}, as follows, Eqs. (1)–(3):

$$\text{l-Lactate} + (LOx)_{ox} \rightarrow \text{Pyruvate} + (LOx)_{red} \quad (1)$$

$$(LOx)_{red} + M_{ox} \rightarrow (LOx)_{ox} + M_{red} \quad (2)$$

* Corresponding authors.
E-mail addresses: vipzanini@hotmail.com (V.I. Paz Zanini), cdborsarelli@gmail.com (C.D. Borsarelli).

http://dx.doi.org/10.1016/j.snb.2017.03.103
0925-4005/

$$M_{red} \rightarrow M_{ox} + e \quad (3)$$

The immobilization of enzyme molecules onto electrode surfaces is one of the most important steps in the construction of a biosensor, being necessary "friendly" methodologies that retain or improve the catalytic properties of the enzyme. In the case of LOx based biosensors, different strategies have been used [2], such as incorporation into mesoporous silica matrices containing cobalt phthalocyanine [12], sol-gel film on multi-walled carbon nanotubes/platinum nanoparticles [13], laponite hydrogels [14,15], covalent attachment to thiols [16,17], and layer-by-layer assembly with polydiallyldimethylammonium chloride (PDDA) and MnO_2 nanoparticles [18]. In particular, the layer-by-layer (LbL) self-assembly technique allows a rational design of multilayered architectures in a simple and reproducible way, with efficient immobilization of enzymes and also nanoparticles (NP) [19,20]. The incorporation of the latter into these supramolecular assemblies usually produces superior catalytic and sensing properties. For this purpose, gold nanoparticles (AuNP) are very suitable nanomaterials due to their excellent biocompatibility, large specific surface area, and electrical conductivity [21,22]. These features provide an appropriate nano-environment with larger exposed surface for the immobilization of active enzymes, enhancing the electronic coupling between the enzyme and the electrode [21,23–26]. Moreover, it has been shown that the incorporation of metal NP in the immobilization matrix leads to a broader enzymatic working pH and temperature range, in comparison with the native enzyme [19].

Considering the above results, in the present work we extended our study on bioelectrodes containing LOx [10,14,15], characterizing an L-lactate amperometric biosensor made with a layer-by-layer (LbL) film composed of PDDA/AuNPs/LOx supported onto a thiol-modified polycrystalline gold electrode (PGE) surface. The interaction of AuNP with PDDA was also analyzed by absorption spectroscopy both in aqueous solution and at a quartz surface. The electrochemical properties of the bioelectrode have been characterized by chronoamperometry (CA), cyclic voltammetry (CV) and electrochemical impedance spectroscopy (EIS). Finally, the electroanalytical performance of the biosensor was evaluated for determination of L-lactate in standard solutions and also in commercial dairy products, and the effect of common interfering compounds were also analyzed. The presented results confirmed the suitability of this supramolecularly assembled bioelectrode for the fast quantification of L-lactate in dairy products.

2. Experimental

2.1. Reagents and materials

Lactate oxidase (LOx, EC 232-841-6 from *Pediococcus* species) 20 units.mg^{-1} solid, citrate buffer-stabilized gold nanoparticles (AuNP) of 10 nm diameter (certificated concentration of 4.7 nM), L−(+)-glucose, citric acid, ascorbic acid, polydiallyldimethylammonium chloride (PDDA, MW = 100–200 kDa) 20% aqueous solution, 3-mercapto-1-propane sulfonic acid sodium salt (MPS), ferrocene methanol (FcMe), potassium ferricyanide and ferrocyanide ($K_3[Fe(CN)_6]$ and $K_4[Fe(CN)_6]$) and L-(+)-lactic acid lithium salt 97% were purchased from Sigma-Aldrich. Phosphate sodium salts NaH_2PO_4 and Na_2HPO_4, and sodium hydroxide were reagent grade from J. T. Baker (Mexico D.F.). Organic solvents such as acetic acid and ethanol were analytical grade (Cicarrelli SRL, Argentina). Solutions were prepared from Milli Q (Millipore) deionized water. Compressed ultrapure N_2 (99.99%) was purchased from Indura SRL (S.M. de Tucumán, Argentina).

2.2. Electrochemical measurements

Cyclic voltammetry (CV), electrochemical impedance spectroscopy (EIS) and chronoamperometry (CA) studies were carried out with the Autolab system equipped with a PGSTAT 30 potentiostat and GPES/FRA 4.9 software package (Eco-Chemie, Utrecht, Netherlands). Working electrodes were prepared by modification of polycrystalline gold electrode (PGE) of 2 mm diameter. A large-area platinum wire was employed as a counter electrode. All potentials are reported against the reference electrode Ag|AgCl|Cl$^-$ (3 M). CA measurements were registered at 400 mV under convective conditions in N_2-satured solutions by gas bubbling during 30 min prior to each measurement. In turns, EIS measurements were carried out in 5 mM $K_3[Fe(CN)_6]$ + 5 mM $K_4[Fe(CN)_6]$ prepared in 0.1 M KCl. Amplitude of the alternate voltage was 10 mV at a bias potential of 200 mV and frequency range 0.05 Hz–10 kHz.

Zeta-potential measurements of the AuNP solutions in citrate was measured with a SZ-100 Nanopartica instrument (Horiba, USA)

All experiments were carried out at room temperature by triplicate and reported results are presented with their respective standard deviations.

2.3. Preparation of composite multilayer films onto quartz surfaces

Supramolecular films containing PDDA, AuNP and LOx were build up by layer-by-layer (LbL) methodology [27], on the inner faces of modified quartz cuvette according to previous report [28]. Afterwards, a 0.2% w/v PDDA in 0.1 M phosphate buffer pH 7.0 was placed in the treated quartz surface in order to deposit the polycation by electrostatic interactions with the negatively charged surface. The LbL film was completed by alternated immersions of solutions containing AuNP and LOx (2 mg/ml), respectively. The dipping times used for adsorption of PDDA and LOx were 20 min and 30 min, respectively [29]. For the adsorption of AuNP, the optimal adsorption time of 60 min was determined by monitoring the increment of the absorbance of the surface plasmon resonance (SPR) band using a Agilent 8453 spectrometer (Palo Alto, CA, USA).

2.4. Preparation of composite multilayer films onto gold surfaces

Previous to the preparation of the composite multilayer film, the surface of the PGE was polished with alumina powder as described elsewhere [29]. A roughness factor (real area/geometric area) of 3.8 ± 0.4 was determined by cyclic voltammetry at 100 mVs^{-1} considering that the reduction of the gold oxide monolayer requires a charge of 420 μC.cm^{-2} [29]. Subsequently, the Au surface was thiolated by immersion during 30 min into a 0.02 M MPS prepared in 0.016 M H_2SO_4 [30]. After thoroughly rinsing of the PGE/MPS modified electrode with ultra-pure water, the LbL film was prepared by deposition of PDDA, AuNP and LOx, as described in the previous section.

2.5. L-lactate determinations in dairy products

Yogurt and fermented milk samples were diluted with phosphate buffer solution (0.1 M pH 7.0), 1:2 and 1:5 respectively; and afterwards added to 5 mL of the same buffer containing 0.2 mM FcMe. Analyte concentrations were determined by the standard addition method. The amperometric determinations were validated with a standard spectrophotometric method based on the absorbance at 340 nm of NADH formed in the presence of L-lactate by L-lactate dehydrogenase (Boehringer Mannheim/R-Biopharm, Cat. No. 10139084035, ISO 8069:2005).

3. Results and discussion

3.1. UV–vis absorption characterization of the composite multilayers

Fig. 1a shows the absorbance changes of the surface plasmon resonance (SPR) band of AuNP stabilized with citrate buffer solution placed into a quartz cuvette with internal faces modified with an adsorbed PDDA monolayer. The absorption spectra were registered as a function of the contact time t_c with an aqueous stock solution of AuNP (c_{AuNP} = 4.7 nM) and after rinsing with ultra-pure water to remove the non-adsorbed AuNP. The SPR band of AuNP aqueous solution (blue-shaded spectrum) shows the typical absorption maximum at 517 nm corresponding to spherical gold nanoclusters of ≈10 nm diameter [31]. However, after contact with the modified quartz surface a red-shifted and broader SPR band was observed. This spectral distortion was produced by electrostatic binding of the AuNP onto the positively charged quartz surface, since the Zeta-potential value of the AuNP measured in citrate buffer was -63 ± 3 mV. The adsorption kinetics monitored by the absorbance increases of the SPR band of AuNP followed a first-growth kinetics with a lifetime of 59 ± 3 min, reaching a plateau above 200 min (Inset of Fig. 1a). This saturation time value was similar to those observed for the adsorption kinetics of AuNP onto different type of surfaces immersed in solutions with similar initial concentration in the nanoparticle solutions than the used in the present work [25,32].

Due to the simple rate law for the adsorption kinetics, it can be assumed that the adsorption process of AuNP is mainly governed by the diffusion of the nanoparticle, *i.e.* D_{AuNP}. For diffusion controlled adsorptive processes of unstirred solutions to planar adsorbing surfaces, the surface coverage, Γ, is proportional to the square root of the adsorption of contact time t_c, Eq. (4) [33]:

$$\Gamma = 2c_0(D_{AuNP}/\pi)^{1/2}t_c{}^{1/2} \quad (4)$$

This equation implies that for the early stages of the adsorption, every AuNP that touches the quartz surface modified with PDDA sticks on it. As no self-interactions between neighboring adsorbed AuNP are produced, Γ values can be calculated from the SPR absorbance of the AuNP (Supplementary Material). From the linear regression of the calculated data with Eq. (4), the bulk diffusion coefficient $D_{AuNP} = 5.1 \times 10^{-11}$ m^2 s^{-1} for AuNP was calculated from the slope value. This D_{AuNP} value is close to the one calculated from the classical Stokes-Einstein equation for spherical AuNP with radius of 5 nm, *i.e.* $D = kT/6\pi\eta r$ [32], 4.9×10^{-11} m^2 s^{-1}, confirming the diffusional control of the adsorption process.

Similar band red-shifting and broadening that in the case of the adsorption process were observed by adding PDDA to the aqueous dispersion of AuNP, but in this case the spectral changes were dependent on the polycation concentration (Fig. S1, Supplementary Material). To compare the spectral changes of the SPR band obtained in each case, the variation of absorbance ratio A_{600}/A_{517} was evaluated as a function of either t_d or PDDA concentration (Fig. 1b). For the adsorption of AuNP onto the PDDA layer, the ratio A_{600}/A_{517} increased suddenly with t_d up to a constant value of around 0.6, confirming that the spectral distortion of the SPR band was independent on the concentration of adsorbed AuNP. Conversely, for the AuNP dispersed in water, the increment of polycation concentration produces a maximum value of A_{600}/A_{517} at 1.5% PDDA, where the largest distortion of the SPR band was produced (Fig. S1, Supporting Material). However, with extra amounts of PDDA the ratio A_{600}/A_{517} was also constant and closer to 0.6. The position and shape of the SPR band of AuNP is very sensitive to several factors, including self-aggregation [31,32,34] or changes of the surrounding nano-environment of the AuNP [31,35]. Under AuNP aggregation conditions, in-plane self-interactions are certainly stronger than the coupling with the surrounding medium. In such a case, a large modification of the SPR band with the appearance of intense absorbance bands above 600 nm due to new longitudinal light absorption modes is produced [31,36]. In the present case, the AuNP in-plane self-interactions are ruled out, since the SPR band did not change with t_c during the adsorption kinetics of AuNP onto the PDDA layer (*i.e.* A_{600}/A_{517} was constant), confirming that only AuNP-PDDA interactions were occurring as the amount of adsorbed AuNP was increased. Thus, the spectral distortion of the SPR band of the adsorbed AuNP can be assigned to the local change of dielectric constant produced by the positive charged PDDA monolayer, as it has been previously observed for AuNP adsorbed onto both PDDA [24] and quaternized chitosan [22] based multilayers.

On the other hand, the dependence of the spectral shape of the SPR band of aqueous AuNP suspension with the polycation concentration can be the result of the formation of different types of AuNP-PDDA aggregates. Up to 1.5% w/v PDDA the largest spectral distortion of the SPR band was detected; and further addition of polycation produced a SPR absorption band similar to that observed for the AuNP adsorbed onto PDDA monolayer (Fig. 1b). This behavior in solution can be interpreted by the change of the electrostatic balance produced by the interaction of the negatively charged nanoparticles and the polycation molecules. The addition of polycation until 1.5% w/v produces the progressive electrostatic neutralization between AuNP and PDDA favoring the formation of supramolecular aggregates. Above this concentration, polycation excess induces electrostatic repulsion in these aggregates rendering AuNP-PDDA adducts with similar spectral properties than those observed for the adsorbed AuNP onto PDDA monolayer (Fig. 1b).

Fig. 2 compares the UV–vis absorption spectra of up to four (i.e. n = 1–4) multilayer films made of $(PDDA/AuNP/LOx)_n$ onto the internal faces of a quartz cuvette, as described in section 2.3. As both the enzyme and the polycation are transparent above 300 nm, the incorporation of AuNP after each dipping cycle was easily monitored by the absorbance increase of the corresponding SPR band. The inclusion of LOx in the multilayers almost did not changed the SPR band of adsorbed AuNP, suggesting that the enzyme does not largely modify the nano-environment sensed by the AuNP [24]. Nevertheless, as the number of multilayers was increased, the SPR band maximum was shifted from 525 nm to approximately 549 nm (Fig. 2). The good linear increment of the SPR absorbance at 549 nm with the number of deposited multilayers indicates an additive and uniform adsorption of AuNP (inset a of Fig. 2). Furthermore, the absorbance ratio A_{600}/A_{549} was almost constant after the formation of the second multilayer (inset a of Fig. 2). These results can be associated with a "sandwich-like" supramolecular assembly of the adsorbed multilayers that does not modify significantly the nano-environment sensed by the AuNP [24]. To confirm this behavior, the inset b of Fig. 2 compares the SPR bands of AuNP dispersed in water with different amount of PDDA (Fig. S1, Supporting Material) after baseline correction by subtraction of the sample scattering assuming a quadratic polynomial dependence with wavelength. It can be observed that both absorption maximum and band shape of the coiled AuNP-PDDA aggregates obtained with 1.5% w/v PDDA are almost the same that those for the adsorbed multilayers at $n \geq 2$, while for the suspension with 3.0% w/v PDDA the same spectrum was observed than for the first adsorbed multilayer. Thus, under the present experimental conditions, it can be expected a "sandwich-like" supramolecular assembly where AuNP are intercalated between the PDDA and LOx layers without strong inter-nanoparticle interactions.

The estimation of the surface coverage Γ by AuNP after the formation of each multilayer composed by $(PDDA/AuNP/LOx)_n$ was performed using the same procedure than for the PDDA/AuNP bilayer onto quartz surface (see previous section). The calculated

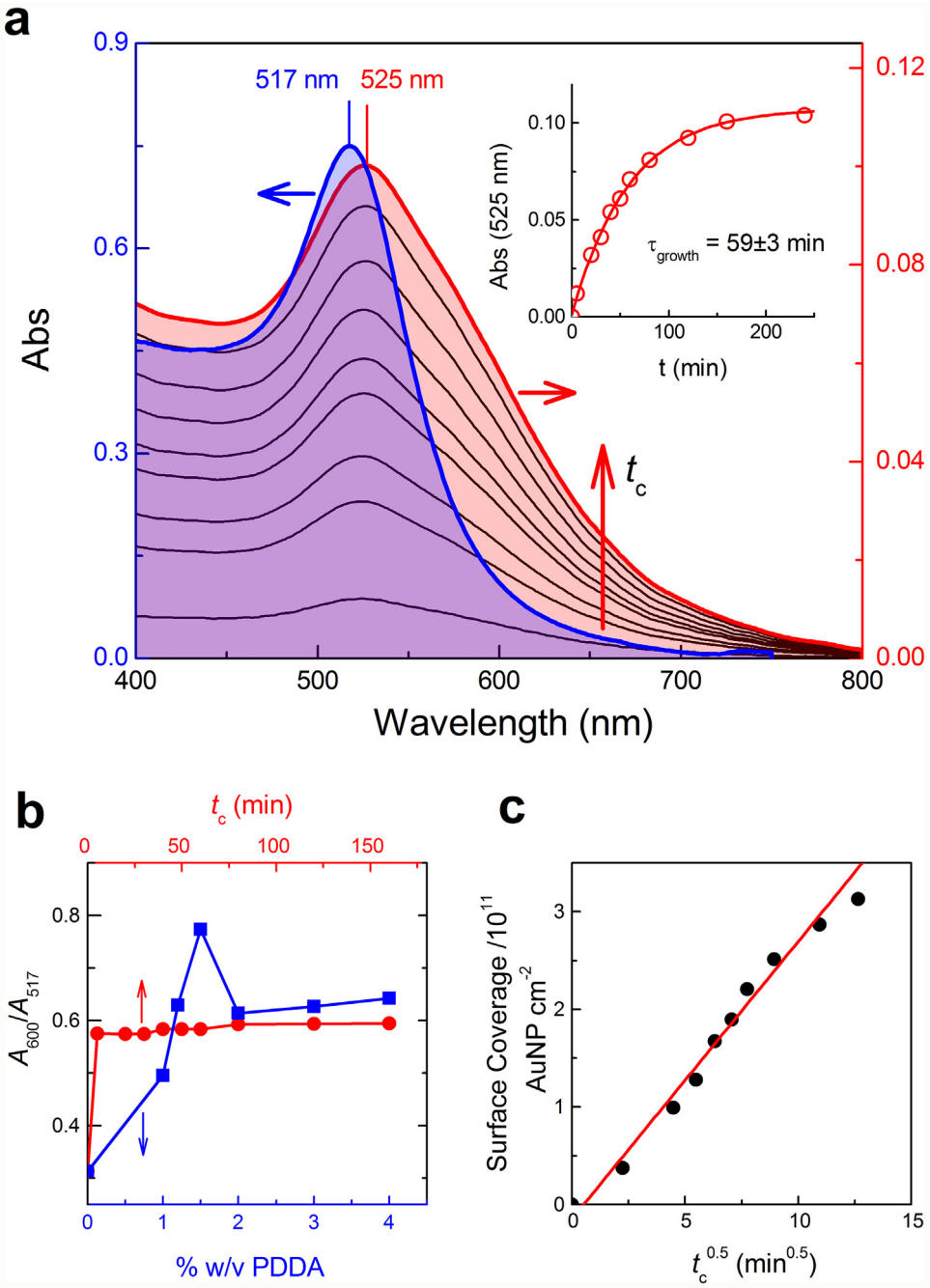

Fig. 1. (a) Absorption spectra of the surface plasmon resonance (SPR) band of AuNP dispersed in water (blue-shaded spectrum) and during adsorption onto a PDDA modified quartz surface (red-shaded spectra) as a function of the contact time t_c (0–160 min). Inset: Adsorption kinetics for AuNP onto PDDA monolayer. (b) Variation of the SPR absorbance ratio A_{600}/A_{517} for adsorbed AuNP onto PDDA modified quartz surface as a function of t_c and for bulk solutions at different PDDA concentration. (c) Dependence of surface coverage Γ with the square root of the dipping time, Eq. (4).

Γ values increased from 2.6×10^{11} to 4.1×10^{11} AuNP per cm^2 between the 1st to the 4th multilayer, respectively. Hence, taking into account that the projected area of a spherical adsorbed nanoparticle of 10 nm diameter is about 7.8×10^{-13} cm^2, the percent of surface coverage increased approximately from 20% for the 1st multilayer to 33% for the 4th multilayer, respectively. For AuNP of different symmetries producing 1:1 distance/diameter ratio the highest percentage of coverage that can be reached is about 55%, due to repulsive interactions among nanoparticles [37]. Indeed, the previous reported values confirm this fact, since a coverage of 22% and 25% has been informed for AuNP deposited on poly(allylmine hydrochloride) [37], and on silicon wafers derivatized with (3-aminopropyl) triethoxysilane [38], respectively.

The coverage values obtained in the present system are similar to those found the formation of the 1st to 4th PDDA/AuNP bilayers in multilayer assemblies without insertion of enzymes, e.g. 19% and 43% respectively [22]. Comparing both sets of data for the 4th multilayers, the lower nanoparticle coverage for assemblies containing LOx can be the result of the total negative charge of the enzyme at neutral pH that competes with the negatively charged AuNP for the adsorption sites at the polycation.

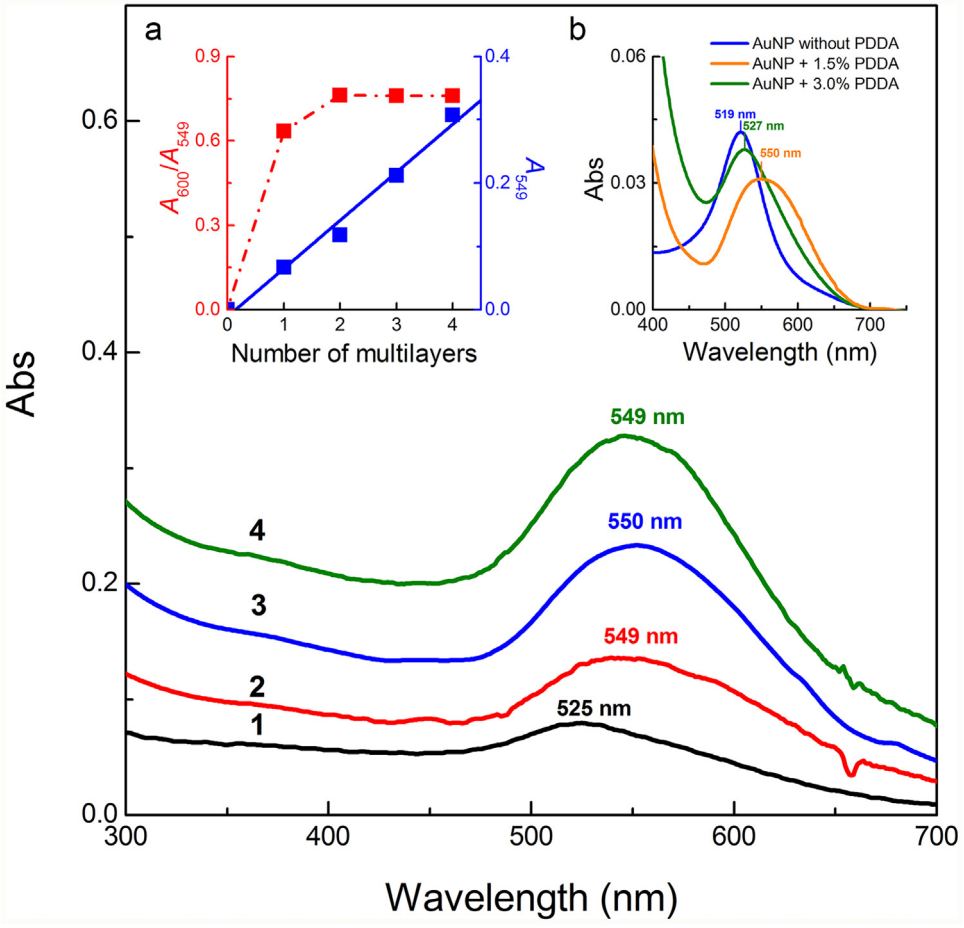

Fig. 2. UV–vis absorption spectra for thin films on quartz surface composed by $(PDDA/AuNP/LOx)_n$ multilayers with n = 1–4. Insets: (a) SPR absorbance at 549 nm and A_{600}/A_{549} ratio for adsorbed AuNP as a function of the number of multilayers. (b) Comparison of the absorption spectra of SPR of AuNP dispersed in water with different amount of PDDA after baseline scattering subtraction with a quadratic polynomial function.

3.2. *Influence of multilayer component on the modified electrode performance*

The conductive features of the PGE modified with the composite multilayers were studied by EIS and CV using $Fe(CN)_6^{3-/4-}$ and FcMe as redox probes, respectively.

Fig. 3a displays the Nyquist plots for the modified electrode after each adsorption step. The impedance curves were well-fitted (solid lines in Fig. 3a) using the classical Randles circuit model (Fig. 3b). The calculated parameters are reported in Table S1 of Supplementary Material. The relevant recovered parameter is the charge-transfer resistance (R_{ct}), which is related with the diameter of the semi-circle obtained at high frequencies of the impedance plots. Thus, larger values of R_{ct} mean a major kinetic inhibition of the electron-transfer process induced by the components of the multilayer system [39]. The sequential changes observed for R_{ct} as function of the electrode composition are explained in terms of the electrostatic interactions between the negatively charged species of the mediator and the different outer layers at the electrode surface, except for the AuNP layer. The decrease in R_{ct} after the AuNP incorporation in the film confirms the role of the gold nanoparticles in enhancing the electron transfer rate of the redox couple [40]. For a system with single electron-transfer kinetics and free of mass-transport complications, as it is given by enough separation in frequencies between kinetic and mass-transport effects, the R_{ct} value is related with the standard heterogeneous rate constant k^0 by Eq. (5) [41]:

$$k^0 = \frac{RT}{F^2 A c R_{ct}} \quad (5)$$

where R is the universal constant of ideal gases, T is the absolute temperature, n the number of electrons transferred, F is the Faraday constant, A is the total electrode area, and c is the molar concentration of redox species ($c = c_{ox} = c_{red}$). Fig. 3c shows the variation of k^0 for different compositions of the multilayer onto the electrode, which are considered as "apparent" heterogeneous rate constants since depend on the complexity of the electrochemical system (*i.e.* real electro-active area, ion permeability and blocking properties). For the bare PGE, the calculated $k^0 = 3.7 \times 10^{-2}$ cm s^{-1} agrees with those previously reported by Sabatani et al. [42] at similar experimental conditions ($k^0 = 1.9$-5.8×10^{-2} cm.s^{-1}). After incorporation of the MPS layer, k^0 was reduced to 2.5×10^{-3} cm. s^{-1} as consequence of the lower ion permeability of the MPS layer and the electrostatic repulsion to the redox probe $Fe(CN)_6^{3-/4-}$ [30]. The further adsorption of PDDA layer slightly increases $k^0 = 4.2 \times 10^{-3}$ cm s^{-1}, as result of electrostatic attraction towards the redox probe. The incorporation of the AuNP in the multilayer also increases k^0, e.g. 1.1×10^{-2} cm s^{-1}, despite of the negative charge of the colloids, which improve the conductive properties of the composite multilayers films [41]. The incorporation of LOx decreases k^0 one-order of magnitude, a similar reduction was reported by Gamero et al. [17] for LOx adsorption on

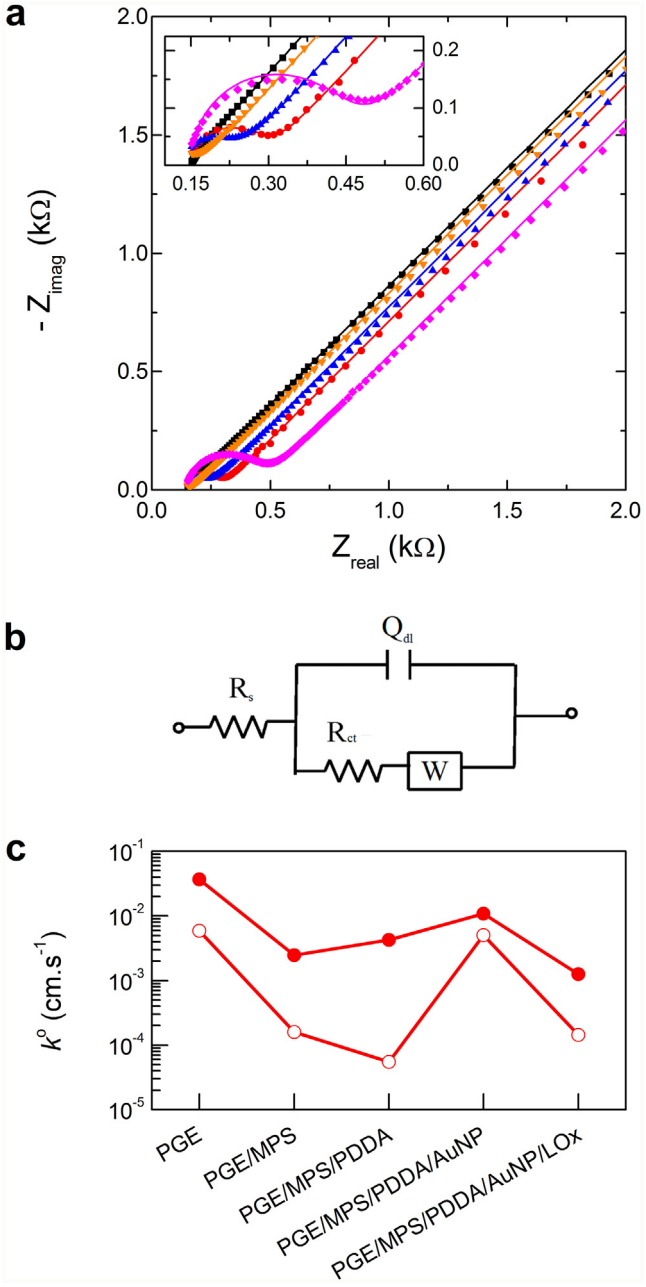

Fig. 3. (a) Nyquist plots for the bare and different modified gold electrodes in the presence of 10 mM $[Fe(CN)_6]^{3-/4-}$ in 0.1 M KCl. (■) PGE, (●) PGE/MPS, (▲) PGE/MPS/PDDA, (▼) PGE/MPS/PDDA/AuNP, and (◆) PGE/MPS/PDDA/AuNP/LOx. Solid lines represent the fitted impedance curves using the Randles circuit. (b) Randles circuit. (c) k^0 for (●) $Fe(CN)_6^{3-/4-}$ and (○) FcMe at different stages of surface modification.

Au-DTSP electrode (gold electrode modified with a self-assembled monolayer of dithiobis-*N*-succinimidyl propionate).

Hence, the overall diffusion coefficient $D = 1.48 \times 10^{-6}\ cm^2\ s^{-1}$ was estimated using Eq. (6) [43], which is a typical value found for this redox probe [44–46],

$$D = \left(\frac{RT\sqrt{2}}{n_e^2 F^2 A c \sigma} \right)^2 \quad (6)$$

where *R*, *T*, *n*, *F*, *A* and *c* are the same as in eq. 4, σ is the frequency dependence of the impedance.

Fig. 4a shows the cyclic voltammograms of 0.2 mM FcMe in 0.1 M phosphate buffer pH 7.0 for the different stages of PGE surface modification. On the bare PGE, the redox couple exhibits the expected reversible behavior for one-electron charge transfer reactions showing a peak separation (ΔE_p) of 65 mV and similar anodic and cathodic peak current values ($|i_{p,a}| \approx |i_{p,c}|$). After consecutive incorporation of MPS and PDDA, the ΔE_p increased to 178 and 237 mV, respectively, and the peak currents i_p decrease sequentially (Fig. 4b). This behavior indicates that the charge reaction of the redox probe is progressively inhibited by the presence of the alkanethiol monolayer and subsequent PDDA adsorption. Mokrani et al. [28] have shown that MPS monolayers are not permeable to FcMe and, on the other hand, repulsive electrostatic interactions have been reported between the positive PDDA outerlayer and the oxidized radical cation ferricinium ($FcMe^{\bullet+}$) [27]. Indeed, the charge effect is more evident for the reduction reaction ($|i_{p,c}| < |i_{p,a}|$) because of the radical cation $FcMe^{\bullet+}$ species have to diffuse to a lesser permeable (PGE/MPS) or positively charged surface (PGE/MPS/PDDA). The AuNP inclusion into the multilayers reset both ΔE_p and i_p to almost the values obtained for bare PGE. Otherwise, the enzyme adsorption increased again ΔE_p and decreased i_p confirming its immobilization. In addition, similar i_p values were obtained for the composite multilayer (PGE/MPS/PDDA/AuNP/LOx).

Additionally, the k^0 values for FcMe (hollow circles in Fig. 3c) were calculated from the CV results employing the Nicholson

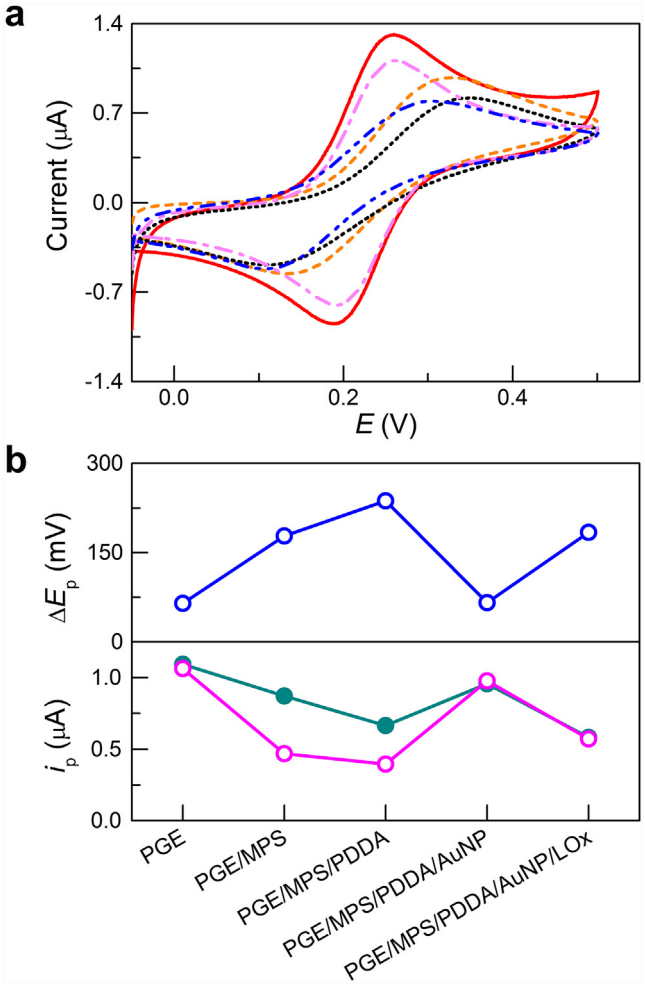

Fig. 4. (a) Cyclic voltammograms obtained at scan rate of 50 mV s^{-1} of 0.2 mM FcMe (in 0.1 M phosphate buffer pH 7.0) with: (_) PGE, (...) PGE/MPS, (·····) PGE/MPS/PDDA, (_ _) PGE/MPS/PDDA/AuNP, and (-·-·-·-) PGE/MPS/PDDA/AuNP/LOx. (b) Peak separation, ΔE_p and peak current, i_p, variations for the different stages (oxidation: ●; reduction: ○).

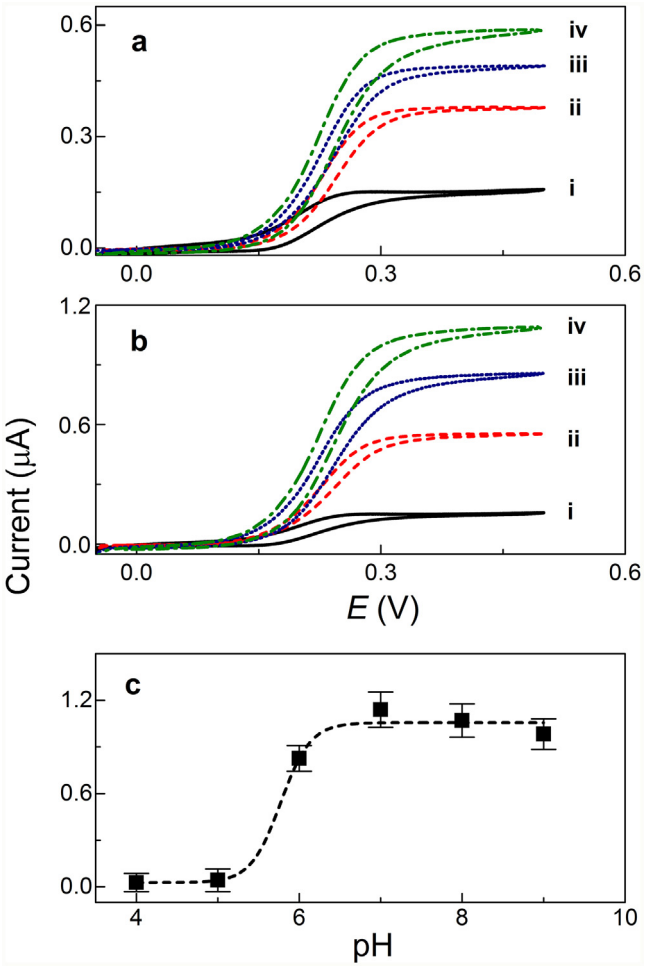

Fig. 5. Cyclic voltammograms of (a): PGE/MPS/$(PDDA/LOx)_n$; and (b): PGE/MPS/$(PDDA/AuNP/LOx)_n$ in 0.1 M phosphate buffer solution, pH 7, containing 0.2 mM FcMe in the absence (i) and presence (ii, iii, iv) of 0.2 mM L-lactate, where n denotes the number of multilayers, n = 1 (i, ii), 2 (iii), 3 (iv). Scan rate 1 mV s^{-1}. (c) Effect of solution pH on the response of PGE/MPS/$(PDDA/AuNP/LOx)_3$ in presence of 0.2 mM L-lactate.

[47] and Lavagnini [48] procedures as described in Supplementary Material. Despite of the different k^0 values for $FcMe^{\bullet+}$/FcMe and $Fe(CN)_6^{3-/4-}$ (see Table S2), the variation of k^o with the multilayer composition was similar for both redox probes (Fig. 3c), indicating that the electron charge transfer is only controlled by the surface properties (*i.e.* charge, permeability, conductivity) at each modification stage and not by the charge of the redox probe.

3.3. Electrocatalytic behavior of the PDDA/AuNP/LOx films towards L-lactate oxidation

Fig. 5a and b compare the cyclic voltammograms of 0.2 mM L-lactate with the presence of 0.2 mM FcMe as enzymatic mediator in 0.1 M phosphate buffer pH 7.0 for the PGE/MPS/PDDA/LOx without and with the presence of AuNP, respectively. In all the cases, when the L-lactate was added to the solution, well defined sigmoidal catalytic waves were obtained as result of the reactions described in equations 1–3 (Fig. 5a and b, curves ii, iii, and iv). The catalytic current was increased with the number of adsorbed enzyme layers, and in the presence of AuNP an extra 2.5-times increment of the catalytic current was obtained. This result could be attributed to the well-recognized AuNP properties, such as large specific surface area, reduction of the effective electron transfer distance [49], and excellent biocompatibility [23].

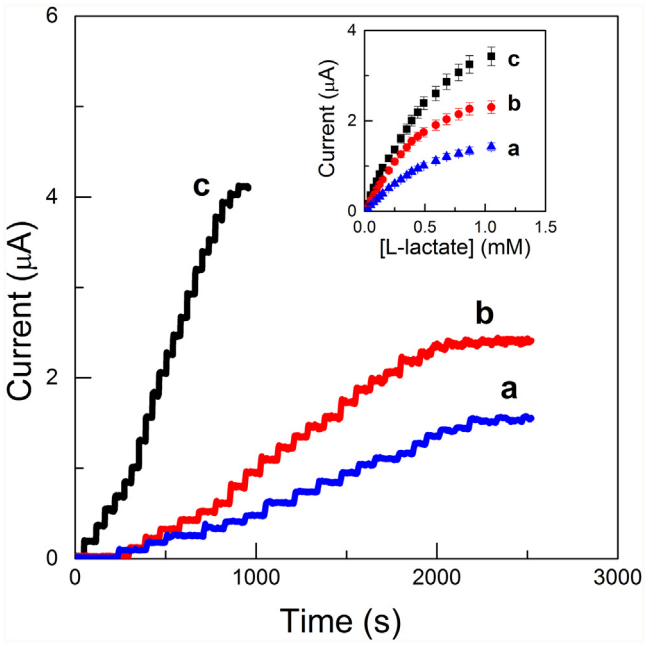

Fig. 6. Amperometric response at 400 mV on PGE/MPS/$(PDDA/AuNP/LOx)_n$, with n = (a) 1, (b) 2 and (c) 3, for successive additions of L-lactate to 0.1 M phosphate buffer pH 7.0 with 0.2 mM FcMe. Inset: Calibration plots of the respective amperometric curves.

The effect of the pH solution on the catalytic current for PGE/MPS/$(PDDA/AuNP/LOx)_3$ shows that at pH > 6 the enzymatic activity was optimal, in agreement with [12,15,50], confirming the biocompatibility of the multilayer.

3.4. Electroanalytical performance of the biosensor

Fig. 6 shows typical current-time plots obtained with PGE/MPS/$(PDDA/AuNP/LOx)_n$ upon successive additions of L-lactate. For all multilayers films, well-defined steady-state current with response time around 10–12 s was observed, indicating that, regardless of the number of layers, the films are perfectly permeable to reagents and products of the enzymatic reaction. Multilayers films sensitivities (26 ± 3, 47 ± 4 and 63 ± 3 μA mM^{-1} cm^{-2}, for n = 1, 2 and 3; respectively) confirm that the catalytic activity increase with the number of enzyme layers, but not linearly. This might suggest that the same amount of enzyme is not adsorbed in each layer or that the lower layer enzyme molecules are not all available. Moreover, the linear range is the same for all films (up to 0.25 mM), indicating that the limiting step is the enzymatic reaction [51]. Considering these facts, and the balance of electrode time preparation/sensitivity obtained, we choose the bioelectrode with three enzyme layers for the analytical porpoises. Table 1 compares the analytical parameters of PGE/MPS/$(PDDA/AuNP/LOx)_3$ with others bioelectrodes (with different surface modification) previously reported in literature.

The K_M^{app} value, calculated accordingly to Eadie-Hofstee plot (Fig. S2, Supplementary Material) $(4.4 \pm 0.2) \times 10^{-4}$ M, was close to the one for the free enzyme [52], 2.3×10^{-4} M, confirming that no significant conformational changes occurred as a result of enzyme immobilization into the composited multilayer.

The reproducibility of the measurement was evaluated by determining the sensitivity of five successive amperometric calibrations assays, using the same electrode surface, obtaining a relative standard deviation (R.S.D.) of 6%. On the other hand, the reproducibility between three bioelectrode prepared from the same batch of solutions, yielded also R.S.D. of 6%. Furthermore, the evaluation of

Table 1
Electroanalytical properties of different modified electrodes containing immobilized Lactate oxidase (LOx).

Modified electrode	Linear range (mM)	Detection limit (μM)	Sensitivity (μA mM^{-1} cm^2)	Electroactive species	Response time (s)	Ref.
PGE/PDDA/AuNP/LOx	0.001–0.25	0.47 ± 0.09	63 ± 3	FcMe	<10	This work
Au/LOx	0.03–0.3	10	3.8 ± 0.4	HMFc	–	[52]
Au/DTSP/LOx	0.12–0.2	40	3.4 ± 0.4	HMFc	–	[52]
Au_R/DTSP/LOx	0.007–1.2	2.2	0.38	HMFc	–	[17]
Au_{3DOM}/LOx	0.049–0.6	16.2	0.73	HMFc	–	[53]
Au_{3DOM}/DTSP/LOx	0.012–1.3	3.9	1.51	HMFc	–	[53]
Albumin and mucin hydrogel	0.002–1	0.8	17.1 ± 0.2	H_2O_2	50	[54]
PtNP/CNF/PDDA	0.025–1.5	11	36.8	H_2O_2		[55]
Mesoporous silica/Co phthalocyanine	0.05–1.5	18.3	4.54	H_2O_2	90	[12]
Polyaniline-co-fluoroaniline film	0.1–5.5	100	1.18	H_2O_2	–	[56]
Carbon paste modified with Niobium oxide	0.1–5.5	0.65	1	H_2O_2	–	[57]
α-MoO_3 nanowire	0.5–8	150	12.43	H_2O_2	10	[58]
Poly- L-Lysine/poly(4-styrenesulfonate)	3×10^{-4}–0.3	0.1	68	H_2O_2	5	[59]

Detection limit was calculated as 3.3σ/*S*, where σ is the standard deviation of the blank signal and *S* the sensitivity [60].
DTSP: 3,3′-dithiopropionic acid di(*N*-succinimidyl ester).
Au_R: Rough gold surface.
Au_{3DOM}: Three-dimentional ordered.

stability of the modified PGE indicated that ≈85% and ≈50% of the initial sensibility was preserved after 10 and 30 days, respectively. (Fig. S3, Supplementary Material).

3.5. L-lactate determination in real samples

The modified bioelectrode PGE/MPS/(PDDA/AuNP/LOx)$_3$ was also used for the quantification of L-lactate in yogurt and fermented milk. Previously, the possible interference of other compounds presented in dairy products matrix such as glucose and citric, acetic and ascorbic acids [53] was also analyzed using amperometry. Each potential interfering compound was added to the electrochemical cell containing 0.2 mM FcMe + 0.1 mM L-lactate, at a molar ratio [interferent]/[L-lactate] = 20. None of the analyzed substances, except ascorbic acid (AA), presented electrochemical response at the biosensor. Nevertheless, the AA/L-lactate molar concentration ratio in real samples is usually <0.001 [10]. Moreover, considering the previous dilution performed in real samples, the AA concentration in the electrochemical cell is about 10 nM, while the detection limit for AA on the modified electrode was 7 μM as calculated from the corresponding calibration curve (Fig. S4, Supplementary Material). Hence, the interference of AA could be considered negligible.

Before to quantify the L-lactate content in yogurt and fermented milk, possible matrix effects were analyzed in terms of the apparent recovery (R_A), Eq. (6) [54]:

$$R_A = \frac{x(obs, O+S) - x(obs, O)}{x(S)} \quad (6)$$

where $x(obs, O+S)$ is the observed value for the spiked sample, $x(obs, O)$ the observed value for the original, unspiked sample, and $x(S)$ the value for the spike. In separate experiments, three different volumes of each real sample were added to the electrolytic cell previously containing of 0.025 mM L-lactate. Then, an extra aliquot of 0.025 mM L-lactate was added. The R_A values expressed as percentage were of 99%, 93% and 70% for 10, 15 and 30 μL of yogurt and 94%, 90% and 85% for 5, 10 and 25 μL of fermented milk, respectively. Hence, to minimize matrix interference effects, the lowest real sample volume was used for analytical purposes. The average L-lactate levels as the result of three replicates were 69 ± 3 mM and 128 ± 4 mM for yogurt and fermented milk, respectively. These results agree with those determined with a standard spectrophotometric method of 72 ± 3 mM and 131 ± 6 mM for yogurt and fermented milk, respectively.

4. Conclusions

Composite multilayers films of (PDDA/AuNP/LOx) were prepared by means of self-assembled multilayers methodology on quartz and PGE surfaces. Results indicate that AuNP adsorption onto quartz surface was a diffusion-controlled process, without significant in-plane interactions between adsorbed AuNP, and absorbance changes observed in the SPR band were produced by of nano-environment change due to the presence of PDDA at the surface.

The presence of AuNP in the modified PGE improved electroanalytical parameters in relation to those without AuNP, as expected for this type of nanoparticles in hybrid bio-assemblies [55].

Compared to other L-lactate biosensors (Table 1), the PGE/MPS/(PDDA/AuNP/LOx)$_3$, showed a remarkable analytical performance, proving that the proposed films are suitable platforms for LOx immobilization.

The electroanalytical performance of PGE/MPS/(PDDA/AuNP/LOx)$_3$ was appropriate for the selective detection of L-lactate in yogurt and fermented milk, opening the feasibility to use it with other food and beverage matrixes.

Acknowledgments

Authors would like to thank the financial support of the following Argentinean Institutions: Universidad Nacional de Santiago del Estero, CONICET (PIO-UNSE-2014-0012 and 0013) and FONCyT (PICT-2012-2666 and PICTO-UNSE-2012-0013).

Appendix A. Supplementary data

Supplementary data associated with this article can be found, in the online version, at http://dx.doi.org/10.1016/j.snb.2017.03.103.

References

[1] F. Shapiro, N. Silanikove, Rapid and accurate determination of d- and l-lactate, lactose and galactose by enzymatic reactions coupled to formation of a fluorochromophore: applications in food quality control, Food Chem. 119 (2010) 829–833.
[2] L. Rassaei, W. Olthuis, S. Tsujimura, E.R. Sudhölter, A. van den Berg, Lactate biosensors: current status and outlook, Anal. Bioanal. Chem. 406 (2014) 123–137.
[3] F. Leroy, L. De Vuyst, Lactic acid bacteria as functional starter cultures for the food fermentation industry, Trends Food Sci. Tech. 15 (2004) 67–78.
[4] M.P. Milagres, S.C. Cardoso Brandão, M. Araujo Magalhães, V.P. Rodriguez Minim, L.A. Minim, Development and validation of the high performance liquid chromatography-ion exclusion method for detection of lactic acid in milk, Food Chem. 135 (2012) 1078–1082.

[5] M. Przybyt, J. Iciek, A. Papiewska, J. Biernasiak, Application of biosensors in early detection of contamination with lactic acid bacteria during apple juice and concentrate production, J. Food Eng. 99 (2010) 485–490.
[6] L. Saavedra, C. Barbas, Optimization of the separation lactic acid enantiomers in body fluids by capillary electrophoresis, J. Chromatogr. B 766 (2002) 235–242.
[7] N.J. Ronkainen, H.B. Halsall, W.R. Heineman, Electrochemical biosensors, Chem. Soc. Rev. 39 (2010) 1747–1763.
[8] M. Przybyt, Lactate biosensors for food industry, Biotechnol. Food Sci. 78 (2014) 71–78.
[9] K. Rathee, V. Dhull, R. Dhull, S. Singh, Biosensors based on electrochemical lactate detection: a comprehensive review, Biochem. Biophys. Rep. 5 (2016) 35–54.
[10] V.I. Paz Zanini, B. López de Mishima, P. Labbé, V. Solís, An L-lactate amperometric enzyme electrode based on L-lactate oxidase immobilized in a laponite gel on a glassy carbon electrode. application to dairy products and red wine, Electroanalysis 22 (2010) 946–954.
[11] H. Liu, J. Deng, An amperometric lactate sensor employing tetrathiafulvalene in Nafion film as electron shuttle, Electrochim. Acta 40 (1995) 1845–1849.
[12] T. Shimomura, T. Sumiya, M. Ono, T. Ito, T. Hanaoka, Amperometric L-lactate biosensor based on sreen-printed carbon electrode containig cobalt phthalocyanine coated with lactate oxidase-mesoporous silica conjugate layer, Anal. Chim. Acta 714 (2012) 114–120.
[13] J. Huang, J. Li, Y. Yang, X. Wang, B. Wu, J.-i. Anzai, et al., Development of an amperometric l-lactate biosensor based on L-lactate oxidase immobilized through silica sol–gel film on multi-walled carbon nanotubes/platinum nanoparticle modified glassy carbon electrode, Mat. Sci. Eng. C 28 (2008) 1070–1075.
[14] V. Paz Zanini, B. López de Mishima, V. Solís, An amperometric biosensor based on lactate oxidase immobilized in laponite–chitosan hydrogel on a glassy carbon electrode. Application to the analysis of l-lactate in food samples, Sens. Actuatos B-Chem. 155 (2011) 75–80.
[15] V.I. Paz Zanini, F. Tulli, M.D. M, B. López de Mishima, C.D. Borsarelli, Improvement of the amperometric response to L-lactate by using a cationic bioinspired thymine polycation in a bioelectrode with immobilized lactate oxidase, Sens. Actuators B-Chem. 181 (2013) 251–258.
[16] M. Gamero, J.L.G. Fierro, E. Lorenzo, C. Alonso, Electrocatalytic activity of 3-dimensional ordered macroporous gold electrode-based lactate biosensors platforms as a function of pore layer number, Electroanalysis 25 (2013) 179–188.
[17] M. Gamero, F. Pariente, E. Lorenzo, C. Alonso, Nanostructured rough gold electrodes for the development of lactate oxidase-based biosensors, Biosens. Bioelectron. 25 (2010) 2038–2044.
[18] J.-J. Xu, W. Zhao, X.-L. Luo, H.-Y. Chen, A sensitive biosensor for lactate based on layer-by-layer assembling MnO_2 nanoparticles and lactate oxidase on ion-sensitive field-effect transistors, Chem. Commun. (2005) 792–794.
[19] S.A. Ansari, Q. Husain, Potential applications of enzymes immobilized on/in nano materials: a review, Biotechnol. Adv. 30 (2012) 512–523.
[20] J.R. Siqueira Jr., L. Caseli, F.N. Crespilho, V. Zucolotto, O.N. Oliveira Jr., Immobilization of biomolecules on nanostructured films for biosensing, Biosens. Bioelectron. 25 (2010) 1254–1263.
[21] A. Zabet-Khosousi, A.-A. Dhirani, Charge transport in nanoparticle assemblies, Chem. Rev. 108 (2008) 4072–4124.
[22] M.V. Bracamonte, O.E.L. Pérez, M.L. Teijelo, G.A. Rivas, N.F. Ferreyra, Quaternized chitosan mediated assembly of gold nanoparticles multilayers, Electrochim. Acta 146 (2014) 178–185.
[23] W. Yang, J. Wang, S. Zhao, Y. Sun, C. Sun, Multilayered construction of glucose oxidase and gold nanoparticles on Au electrodes based on layer-by-layer covalent attachment, Electrochem. Commun. 8 (2006) 665–672.
[24] M.M. Ottakam Thotiyl, H. Basit, J.A. Sánchez, C. Goyer, L. Coche-Guerente, P. Dumy, et al., Multilayer assemblies of polyelectrolyte–gold nanoparticles for the electrocatalytic oxidation and detection of arsenic(III), J. Colloid Interface Sci. 383 (2012) 130–139.
[25] Z. Qi, I. Honma, M. Ichihara, H. Zhou, Layer-by-layer fabrication and characterization of gold-nanoparticle/myoglobin nanocomposite films, Adv. Funct. Mater. 16 (2006) 377–386.
[26] H.W. Yang, D.C. Kim, S.-H. Yoo, S. Park, D.J. Kang, Constructing LBL-assembled functional bio-architecture using gold nanorods for lactate detection, Mater. Res. Bull. 47 (2012) 3056–3060.
[27] J. Hodak, R. Etchenique, E.J. Calvo, K. Singhal, P.N. Bartlett, Layer-by-layer self-assembly of glucose oxidase with a poly(allylamine)ferrocene redox mediator, Langmuir 13 (1997) 2708–2716.
[28] Y.M. Lvov, G.N. Kamau, D.-L. Zhou, J.F. Rusling, Assembly of electroactive ordered multilayer films of cobalt phthalocyanine tetrasulfonate and polycations, J. Colloid Interface Sci. 212 (1999) 570–575.
[29] N. Ferreyra, L. Coche-Guérente, P. Labbé, Construction of layer-by-layer self-assemblies of glucose oxidase and cationic polyelectrolyte onto glassy carbon electrodes and electrochemical study of the redox-mediated enzymatic activity, Electrochim. Acta 49 (2004) 477–484.
[30] C. Mokrani, J. Fatisson, L. Guérente, P. Labbé, Structural characterization of (3-mercaptopropyl)sulfonate monolayer on gold surfaces, Langmuir 21 (2005) 4400–4409.
[31] S.K. Ghosh, T. Pal, Interparticle coupling effect on the surface plasmon resonance of gold nanoparticles: from theory to applications, Chem. Rev. 107 (2007) 4797–4862.
[32] J. Schmitt, P. Mächtle, D. Eck, H. Möhwald, C.A. Helm, Preparation and optical properties of colloidal gold monolayers, Langmuir 15 (1999) 3256–3266.
[33] H.J. van Enckevort, D.V. Dass, A.G. Langdon, The adsorption of bovine serum albumin at the stainless-steel/aqueous solution interface, J. Colloid Interface Sci. 98 (1984) 138–143.
[34] J. Yuan, A. Hajebifard, C. George, P. Berini, S. Zou, Ordered gold nanoparticle arrays on glass and their characterization, J. Colloid Interface Sci. 410 (2013) 1–10.
[35] S.K. Ghosh, S. Nath, S. Kundu, K. Esumi, T. Pal, Solvent and ligand effects on the localized surface plasmon resonance (LSPR) of gold colloids, J. Phys. Chem. B 108 (2004) 13963–13971.
[36] N. Malikova, I. Pastoriza-Santos, M. Schierhorn, N.A. Kotov, L.M. Liz-Marzán, Layer-by-layer assembled mixed spherical and planar gold nanoparticles: control of interparticle interactions, Langmuir 18 (2002) 3694–3697.
[37] C. Jiang, S. Markutsya, V.V. Tsukruk, Collective and individual plasmon resonances in nanoparticle films obtained by spin-assisted layer-by-layer assembly, Langmuir 20 (2004) 882–890.
[38] E.S. Kooij, H. Wormeester, E.M. Brouwer, E. van Vroonhoven, A. van Silfhout, B. Poelsema, Optical characterization of thin colloidal gold films by spectroscopic ellipsometry, Langmuir 18 (2002) 4401–4413.
[39] V. Pardo-Yissar, E. Katz, O. Lioubashevski, I. Willner, Layered polyelectrolyte films on Au electrodes: characterization of electron-transfer features at the charged polymer interface and application for selective redox reactions, Langmuir 17 (2001) 1110–1118.
[40] H. Zhang, H. Lu, N. Hu, Fabrication of electroactive layer-by-layer films of myoglobin with gold nanoparticles of different sizes, J. Phys. Chem. B 110 (2006) 2171–2179.
[41] A.J. Bard, L.R. Faulkner, Electrochemical Methods, Wiley, New York, 1980.
[42] E. Sabatani, I. Rubinstein, R. Maoz, J. Sagiv, Organized self-assembling monolayers on electrodes. Part I. Octadecyl derivatives on gold, J. Electroanal. Chem. 219 (1987) 365–371.
[43] F.G. Banica, Chemical Sensors and Biosensors, Willey, United Kingdom, 2012.
[44] S.J. Konopka, B. McDuffie, Diffusion coefficients of ferri- and ferrocyanide ions in aqueous media, using twin-electrode thin-layer electrochemistry, Anal. Chem. 42 (1970) 1741–1746.
[45] J.E. Baur, R.M. Wightman, Diffusion coefficients determined with microelectrodes, J. Electroanal. Chem. 305 (1991) 73–81.
[46] T. Gueshi, K. Tokuda, H. Matsuda, Voltammetry at partially covered electrodes. Part III. Faradaic impedance measurements at model electrodes, J. Electroanal. Chem. 102 (1979) 41–48.
[47] R.S. Nicholson, Theory and application of cyclic voltammetry for measurement of electrode reaction kinetics, Anal. Chem. 37 (1965) 1351–1355.
[48] I. Lavagnini, R. Antiochia, F. Magno, An extended method for the practical evaluation of the standard rate constant from cyclic voltammetric data, Electroanalysis 16 (2004) 505–506.
[49] J. Zhao, R.W. Henkens, J. Stonehuerner, J.P. O'Daly, A.L. Crumbliss, Direct electron transfer at horseradish peroxidase—colloidal gold modified electrodes, J. Electroanal. Chem. 327 (1992) 109–119.
[50] G. Aydın, S.S. Çelebi, H. Özyörük, A. Yıldız, Amperometric enzyme electrode for l(+)-lactate determination using immobilized l(+)-lactate oxidase in poly(vinylferrocenium) film, Sens. Actuators B-Chem. 87 (2002) 8–12.
[51] S. Poyard, N. Jaffrezic-Renault, C. Martelet, S. Cosnier, P. Labbe, Optimization of an inorganic/bio-organic matrix for the development of new glucose biosensor membranes, Anal. Chim. Acta 364 (1998) 165–172.
[52] S. Suman, R. Singhal, A.L. Sharma, B.D. Malthotra, C.S. Pundir, Development of a lactate biosensor based on conducting copolymer bound lactate oxidase, Sens. Actuators B-Chem. 107 (2005) 768–772.
[53] B. Serra, A.J. Reviejo, C. Parrado, J.M. Pingarrón, Graphite-teflon composite bienzyme electrodes for the determination of l-lactate: application to food samples, Biosens. Bioelectron. 14 (1999) 505–513.
[54] D.T. Burns, K. Danzer, A. Townshend, Use of the term recovery and apparent recovery in analytical procedures (IUPAC Recommendations 2002), Pure Appl. Chem. 74 (2002) 2201–2205.
[55] J.M. Pingarrón, P. Yáñez-Sedeño, A. González-Cortés, Gold nanoparticle-based electrochemical biosensors, Electrochim. Acta 53 (2008) 5848–5866.
[56] S. Suman, R. Singhal, A.L. Sharma, B.D. Malthotra, C.S. Pundir, Development of a lactate biosensor based on conducting copolymer bound lactate oxidase, Sens. Actuators B 107 (2005) 768–772.
[57] A.C. Pereira, A. Kisner, C.R.T. Tarley, L.T. Kubota, Development of a carbon paste electrode for lactate detection based on meldolas blue adsorbed on silica gel modified with niobium oxide and lactate oxidase, Electroanalysis 26 (2011) 1470–1477.
[58] I. Shakir, M. Shahid, H.W. Yang, S. Cherevko, C.-H. Chung, D.J. Kang, α-MoO3nanowire-based amperometric biosensor for L-lactate detection, J. Solid State Electrochem. 16 (2012) 2197–2201.
[59] F. Mizutani, S. Yabuki, Y. Hirata, Amperometric l-lactate-sensing electrode based on a polyion complex layer containing lactate oxidase. Application to serum and milk samples, Anal. Chim. Acta 314 (1995) 233–239.

Biographies

Veronica Paz Zanini obtained his Ph.D. in Chemistry (2008) from Córdoba National University (Córdoba, Argentina). Currently, she is assistant professor at the Faculty of Agronomy and Agro-industries of Santiago del Estero National University

and assistant Researcher at Argentine Research Council (CONICET). Dr. Paz Zanini research interests are focused on the development of molecular recognition platforms for use in the construction of sensors and biosensors, and design and synthesis of nanomaterials with potential application in the field of electroanalysis.

Omar E. Linarez Pérez obtained his Ph.D. in Chemistry (2006) from Córdoba National University (Córdoba, Argentina). He did a postdoctoral training at the Department of Physical Chemistry, Faculty of Chemical Sciences (Córdoba National University) and at Pontifical Catholic University of Valparaíso (Valparaíso, Chile) focusing on the synthesis and characterization of self-organized nanotubular TiO_2 films. Currently, he is assistant professor at the Faculty of Chemical Sciences of Cordoba National University and adjunct Researcher at Argentine Research Council (CONICET). Dr. Linarez Pérez research interests are focused on the preparation and characterization of nanostructured platforms produced by metal anodization under controlled conditions or molecular modification of metallic surfaces.

Manuel Lopez Teijelo obtained his PhD in Chemistry (1977) from Cordoba National University (Cordoba, Argentina). Currently, he is full professor of Physical Chemistry and Electrochemistry at Cordoba National University and Principal Researcher at Argentine Research Council (CONICET). Dr. Lopez Teijelo was the head of the Department of Physical Chemistry at the Faculty of Chemical Sciences between 1996 and 1998. He was the National Secretary for Argentina of the International Society of Electrochemistry (ISE) between 1994 and 1999, and Vice-President and President of the Iberoamerican Society of Electrochemistry between 2004 and 2008. His research interests are focused on surfaces and nanostructured materials, especially the modification of metallic surfaces by self-assembled monolayers of aromatic thiols and derivatives, and characterization of nanostructured platforms produced by metal anodization of metallic surfaces.

Pierre Labbé is a professor at the Universite Joseph Fourier, Grenoble (France) in the "Ingenierie et Interactions Biomoleculaires" (I2BM) laboratory within the Department of Molecular Chemistry (DCM, UMR CNRS 5250). His current research interest concerns the conception of new biofunctional interfaces and stimuli-responsive materials for diagnostic, therapeutic and analytical applications. This activity is developed in strong synergy with the other activities of the laboratory that bring together the synthesis of molecular recognition systems by chemical engineering of biomolecules (nucleic acids, peptides, oligosaccharides and related bioconjugates) and their applications in the field of life science and nanosciences.

Beatriz López de Mishima obtained his Ph.D. in Chemistry (1972) from Córdoba National University (Córdoba, Argentina). Actually she is an emeritus professor at Santiago del Estero National University and principal researcher of National Council of Scientific and Technical Research (CONICET). She was visiting professor of Hokkaido University, Sapporo, Japan (1986–1987) and Universitat Bonn, Germany (1990–1991). Her field of research is electrochemistry of catalytic reaction.

Claudio D. Borsarelli received his Ph.D. in Chemistry from the University of Rio Cuarto, Argentina, in 1994. During 1995-98 was posdoc researcher at the MPI-Radiation Chemistry in Germany, under the supervision of Prof. Silvia Braslavsky. In 2000 joined to the University of Santiago del Estero, Argentina, to initiate a research group in spectroscopy and photochemistry. In 2008 he received a Georg Forster fellowship from the Alexander von Humboldt foundation to visit the MPI-Biophysical Chemistry of Göttingen, in the Jovinís group. He is currently full Professor and Principal Researcher at Argentine Research Council (CONICET). Currently, he is director of the Institute of Bionanotechnology (INBIONATEC) and his research interests are photochemistry and spectroscopy of proteins, and of nano- and micro-structured photo- and electroactive interfaces.